JOURNAL OF AIRCRAFT
Vol. 30, No. 5, Sept.–Oct. 1993

Unsteady Wing Surface Pressures in the Wake of a Propeller

R. T. Johnston* and J. P. Sullivan†
Purdue University, West Lafayette, Indiana 47906

The unsteady nature of the propeller slipstream interacting with a wing has been studied by flow visualization and unsteady wing surface pressure measurements. Flow visualization was performed by marking the propeller tip vortex with smoke. Unsteady wing surface pressures were measured by traversing a wing instrumented with a chordwise array of 16 microphones in a spanwise direction through the propeller wake. This work yielded information on the motion of the propeller wake as it passes over the wing. At the wing leading edge the propeller tip vortex deformed in a spanwise direction which was attributed to an inviscid interaction. Viscous effects at the leading edge then severed the propeller tip vortex. This severed propeller tip vortex experienced significant spanwise and chordwise displacements while passing across the wing. Axial velocity in the vortex core caused the helical vortex to thicken or stretch near the wing surface. At the trailing edge the misaligned vortex filaments deformed in order to reconnect. Vortex core trajectory on the wing surface as measured from pressure contour plots was seen to vary with wing angle of attack. The magnitude of the wing surface pressure fluctuations decreased in magnitude with distance traveled along the chord.

Nomenclature

AR = wing aspect ratio (span/chord)
C = wing chord
C_p^* = unsteady wing surface pressure coefficient, P_u/q_∞
D = propeller diameter
J = advance ratio, V_∞/nD
n = rotational speed, rps
P_u = unsteady wing surface pressure
q_∞ = freestream dynamic pressure
R = propeller radius
r = radial position measured from propeller center of rotation ($r > 0$ on propeller rotation down side)
T = time
T_w = time for a complete propeller revolution
T^* = nondimensional time of the wake passage, T/T_w
V_∞ = freestream velocity
X = chordwise distance along wing (measured from leading edge)

Introduction

BENEFICIAL effects of the aerodynamic interaction between a propeller and a wing were first noted in the 1940s. The authors report an increase in wing lift and a decrease in wing drag for the tractor configuration and conclude that the unexpected results of the propeller/wing interference require further investigation. With the advent of the jet engine, interest in propeller propulsion waned until fuel shortages in the mid 1970s renewed interest in increasing propulsion efficiency. The Advanced Turboprop Program was initiated by NASA to develop a highly efficient alternative to the turbofan engine.[2] Results from this program managed by NASA Lewis indicate that high-speed propfans can be designed with installed propulsion efficiencies that would be 15% higher than the best advanced turbofan at Mach 0.8 cruise. These advanced propellers must be correctly installed to obtain optimum efficiency.

Presented as Paper 92-0277 at the AIAA 30th Aerospace Sciences Meeting and Exhibit, Reno, NV, Jan. 6–9, 1992; received Feb. 2, 1992; revision received May 23, 1992; accepted for publication May 23, 1992.

*Visiting Assistant Professor. Department of Mechanical Engineering. Member AIAA.
†Professor, School of Aeronautics and Astronautics. Member AIAA.

Computational investigations on propeller/wing interactions predict that significant performance gains are possible by proper integration of components. Kroo[3] studies optimum wing designs for tractor and pusher propeller installations and concludes that the optimum solution for a propeller/wing installation differs greatly from that for a "clean wing" distribution. Miranda and Brennan[4] investigate a wing-tip mounted propeller/wing interaction and predict that the drag for an optimum power-on wing load is 32% lower than that of an isolated elliptically loaded wing with the same lift and aspect ratio.

A joint experimental and computational study of the steady (time-averaged) loads on a propeller/wing combination yields good agreement.[5–8] Witkowski[7] employs actuator disk theory to predict wing drag polars for several experimental configurations. Predictions made by Lee[8] using a vortex lattice model agree with the results from the momentum analysis and the steady-state propeller-wing interaction tests performed by Witkowski. These studies demonstrate that lift enhancement and wing drag reduction are possible with certain geometries of a tractor configuration propeller. The physics of the propeller slipstream swirl recovery by the wing is explained by considering the effect of a propeller wake on an infinite wing. The propeller induces regions of upwash and downwash on the wing due to the swirl in the propeller wake. A negative drag (or thrust) is induced on the wing at 0-deg wing angle of attack (AOA) in both the upwash and downwash regions as the Kutta-Joukowski force is rotated forward. For the infinite wing at positive angles of attack, the propeller swirl yields a net drag reduction due to the beneficial effect in the upwash region, despite an increased sectional wing drag in the propeller region. Wing lift is augmented by the increase in axial velocity in the propeller slipstream.

Several contributions to the subject of propeller/wing aerodynamic interactions study wing surface pressure distributions in the wake of the propeller.[9–11] All look at time-averaged pressure at a number of spanwise sections. In general, mean sectional lift coefficient increases behind the up-going blade and decreases behind the downward-rotation blade. Also noted is that the sectional pressure distributions return to normal outside the slipstream.

Steady and unsteady pressure distributions on a propeller under the influence of the upwash from a straight wind is the focus of work by Heidelberg and Woodward.[12] The pressure instrumented blades are calibrated by varying the inflow angle to an isolated propeller. This information allows the unknown inflow angles to be determined with the wing installed. Wing

installation causes a nearly uniform upwash at the propeller inflow plane, and inflow angle is shown to increase at a rate of 150% of the wing angle of attack.

In order to further understand the unsteady nature of the propeller/wing interaction, a flow visualization study was used as an initial phase. By performing flow visualization, qualitative information about the physical nature of the motion of the propeller tip vortex over the wing could be retrieved. The second phase of the study consisted of unsteady wing surface pressure measurements. Knowledge of the propeller wake gained during flow visualization[13-16] aided in the interpretation of unsteady pressure measurements.

Experimental Apparatus

A vortex of large core was determined to be conducive to good flow visualization and would minimize the spatial averaging by the pressure ports during the planned unsteady pressure measurements. Rotor tip vortices are reported to be approximately 0.1 blade-chords in diameter,[17,18] where the vortex radius is defined as the distance from the center to the point of maximum circumferential velocity. This relationship dictated that a propeller of relatively large chord should be used for this experiment. The propeller consisted of two untwisted constant cross-section blades: the blade chord was 10.16 cm, and the overall propeller diameter was 62.23 cm. Pitch settings of 12 and 16 deg were used during flow visualization; whereas, only the pitch setting of 16 deg was used during the pressure measurements.

The wing was positioned one wing chord length behind the propeller as measured from the propeller $\frac{1}{4}$ chord to the wing $\frac{1}{4}$ chord (see Fig. 1). This wing had a NACA 0012 airfoil section with a 20.32-cm chord. Wing aspect ratios were 9 and 18, during the flow visualization and pressure measurements, respectively. All tests were performed in the open section of the Purdue Aerospace Sciences Laboratory wind tunnel at a freestream velocity of 11.6 m/s and Reynolds number of 170,550 based on the wing chord. The turbulence intensity at the center of the open jet test section is 0.019.[19]

Flow Visualization

Flow visualization of the unsteady propeller/wing aerodynamic interaction was undertaken by marking the propeller tip vortex. The hollow drive shaft, hub, and propeller blades allowed smoke to be introduced into the propeller tip vortex through holes located in the blade tips. Operating the propeller at positive and negative thrust coefficients allowed the effect of vortex rotational direction on the interaction to be investigated. These conditions are referred to as power-output and power-absorbing, respectively. A propeller only operates at a negative thrust (or power-absorbing condition) at landing; however, since the relationship between spanwise vortex motion and vortex rotational direction was of interest, this condition was also studied. The range of advance ratios for flow visualization tests varied from $J = 0.37$ to 1.1

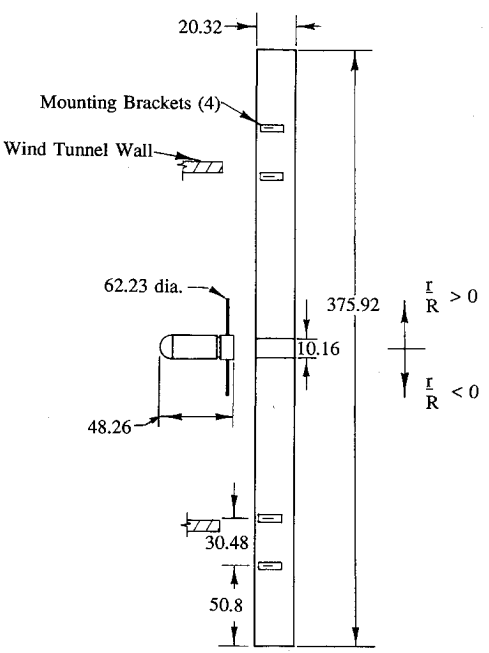

Fig. 1 Plan view of the experimental apparatus used for the unsteady pressure measurements (all dimensions in cm).

Unsteady Pressure Measurement

The low-pressure fluctuations expected during wind-tunnel testing dictated that high sensitivity, high-frequency response pressure transducers be used. Electret microphones were selected for use in the experiment because of their low cost, high sensitivity, and high signal-to-noise ratio. These microphone cartridges have been used for measuring boundary-layer wall pressure fluctuations.[20,21] A Radio Shack minicondenser microphone was selected for use because of its small size (6.0-mm diam) and low cost (under $4.00 per transducer).

A high-quality sinusoidal pressure signal generator was needed for calibration purposes since the frequency response characteristics of the electret microphones were required. An acoustic resonator tube was constructed and checked by comparing the outputs from two B&K 4138 microphones.[15] One B&K microphone was then used as a reference when calibrating each of the electret microphones.

Calibration of these electret microphones over a range from 25 to 6000 Hz revealed that at each individual frequency less than 1.1% error in linearity existed for low pressures but that the sensitivity of the electret microphone varied somewhat over the range of frequency tested. Electret microphone output signals can be corrected using filter coefficients determined by using inverse filtering techniques, but preliminary wind-tunnel testing showed that correction by a calibration constant was acceptable for the frequency content present in the propeller wake.[15] The microphone was tested with and without the factory installed screen. This screen damped the response of the transducer above 4000 Hz and provided protection from damage by foreign objects; thus, it was retained for wind-tunnel testing.

A high aspect ratio wing (AR = 18) was used for the unsteady wing surface pressure measurements. This wing was mounted from an overhead traverse which allowed the instrumented section to be scanned across the wake of the propeller. The wing tips were always located outside the open jet, so the wing vortex sheet roll-up was always located at the edge of the jet. Had the lower aspect ratio wing (AR = 9) been used, the location of the wing-tip vortices would have changed relative to the propeller during pressure measurement surveys, and a variable would have effectively been introduced into the data. Sixteen chordwise pressure ports 0.79-mm in diameter, spaced 1.27-cm apart, were located at the center of the wing span. All electrical connections for these were routed through conduit which had been cast into the wing. The transducer at the trailing edge protruded slightly from the lower surface of the wing due to the reduced thickness in that region and was blended smoothly into the lower wing surface. The chamber behind the transducers was sealed from wind-tunnel pressure fluctuations. Once the electret microphones were installed, in situ calibration was carried out periodically using a B&K 4230 sound level calibrator.

Signals from the transducers were recorded using an R.C. electronics 16 channel A/D board, with an optional simultaneous sample and hold, that was installed in a 286 personal computer. The intersample rate, set at 41×10^{-6} s, yielded 487 data points per revolution with the propeller operating at 50 rps. A total of 510 data points per trace were taken to ensure that data were acquired over a complete revolution. Pressure measurements were synchronized to the propeller in order to allow ensemble averaging. At each spanwise lo-

cation, pressure was measured at 16 locations for 20 complete revolutions. The wing was set to negative AOA to determine the unsteady pressure distribution corresponding to the lower surface of the wing at positive AOA. Pressures measured at negative AOA were assumed to be identical to those on the lower surface at positive AOA. The coordinates of the data taken at negative AOA were then rotated 180 deg about the center of rotation in order to obtain the correct coordinates of the lower surface for plotting. All fluctuating pressure measurements are presented in the coordinate system shown in Fig. 1. Unsteady pressure measurements were obtained for a loaded or power-output condition ($J = 0.37$).

Flow Visualization of the Propeller/Wing Interaction

The propeller/wing interaction flow visualization study revealed details of the propeller tip vortex/solid body interaction. Figure 2 shows a photograph of the apparatus in operation.

When the tip vortex filament approached the leading edge of the wing, an inviscid interaction was evident. As the propeller tip vortex moved toward the wing leading edge it progressively deformed toward the center of rotation in the locality of the leading edge on the rotation-up side during the propeller power-absorbing condition. This bending was attributed to an image vortex effect at the wing leading edge. A view from downstream of this deformation and a two-dimensional image vortex representation are presented in Fig. 3. In the propeller power output case the propeller tip vortex was observed to deform in the direction away from the center of rotation. Viscous effects in the vicinity of the leading edge caused the vortex filament to pinch off and end on the upper and lower wing surfaces (see Fig. 2). These results agree with the smooth body interaction discussed in Quakenbush and Bliss.[22]

Axial velocity in the tip vortex caused the vortex filament to thicken on one side of the wing while it became thinner on the other side. For example, in the propeller rotation-up region, the helical vortex below the wing thickened; whereas, above the wing it appeared to stretch. On the rotation-down side, the vortex thickened above the wing and stretched below the wing. This phenomenon occurred for both the power-absorbing and power-output conditions and was therefore attributed to axial flow in the vortex core (see Fig. 4).

With the wing at 0-deg AOA the filaments appeared to stay aligned and to reconnect relatively cleanly at the trailing edge. Wing AOA was then set to 5 and 10 deg in succession. At both of these angles, noticeable changes were apparent in the motion of the tip vortex. Chordwise misalignment in the tip vortex as the vortex moved along the airfoil was observed. This chordwise misalignment appeared regardless of whether the advance ratio was 0.9 (power-absorbed by propeller) or 0.37 (power-output by propeller) and was attributed to the higher flow velocity above a lifting wing. A spanwise shear or misalignment in the tip vortex while passing the wing at positive angles of attack was also observed. Under power-absorbing propeller conditions ($J = 0.9$), the spanwise shear was outward on the upper surface on the rotation-up side (see Fig. 4). With the propeller producing thrust ($J = 0.37$), the vortex sheared outward below the wing on the propeller rotation-up side. On the propeller rotation-down side, no noticeable spanwise shear was observed under propeller power-output conditions; whereas, the propeller power-absorbing condition exhibited only slight outward movement of the vortex core on the upper surface on the rotation-down side. Displacements in the tip vortex as it passed the wing were observed to increase when wing AOA was increased. Wing AOA was set to -5 deg for the power-absorbing propeller condition, and the spanwise shearing remained the same if the coordinates were rotated 180 deg about the center of rotation. Photographs of the helical vortex after leaving the

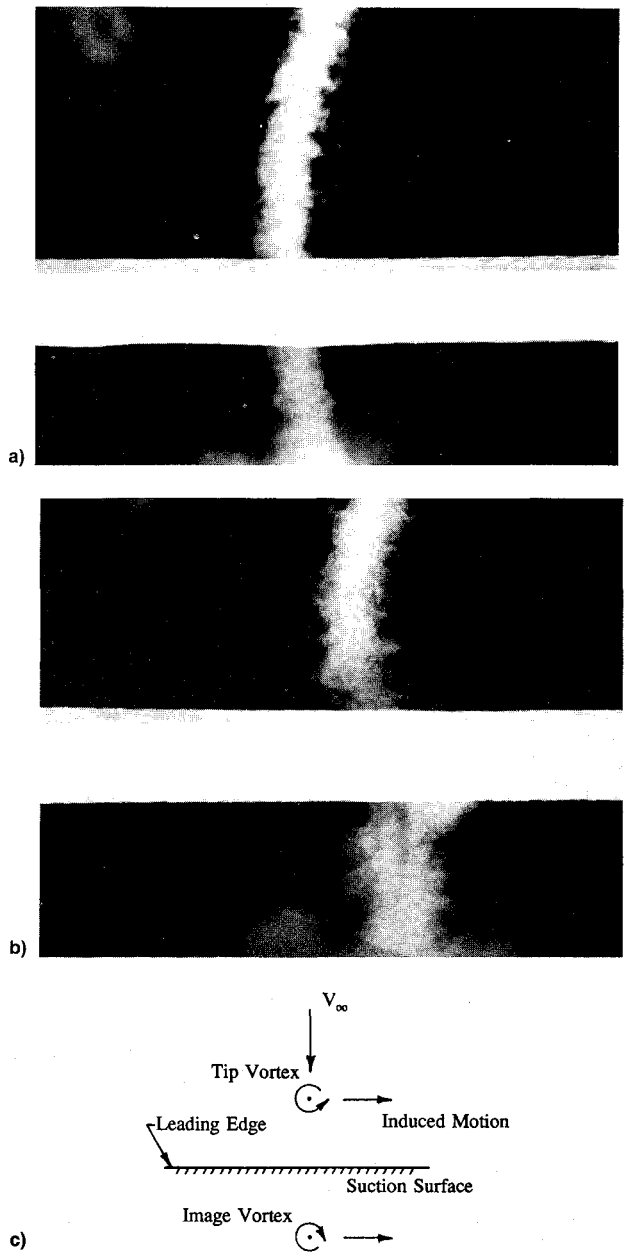

Fig. 3 Tip vortex motion at leading edge for a propeller power absorbing condition (wing AOA = 5 deg, $J = 0.9$): a) tip vortex prior to the leading edge (viewed from downstream); b) tip vortex/leading edge interaction (downstream view); and c) plan view of wing and two-dimensional image vortex representation.

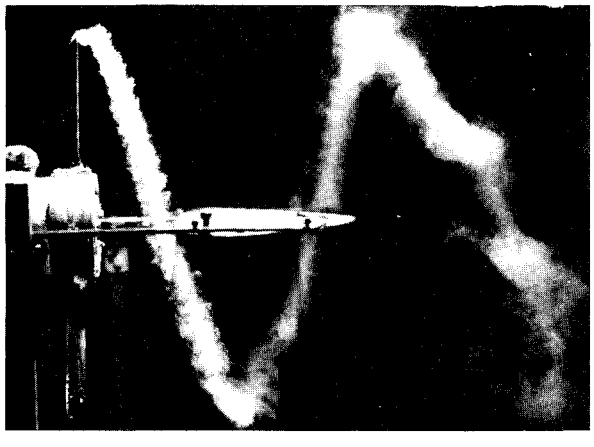

Fig. 2 Side view of the propeller-wing apparatus in operation (blade pitch = 12 deg, $J = 0.9$).

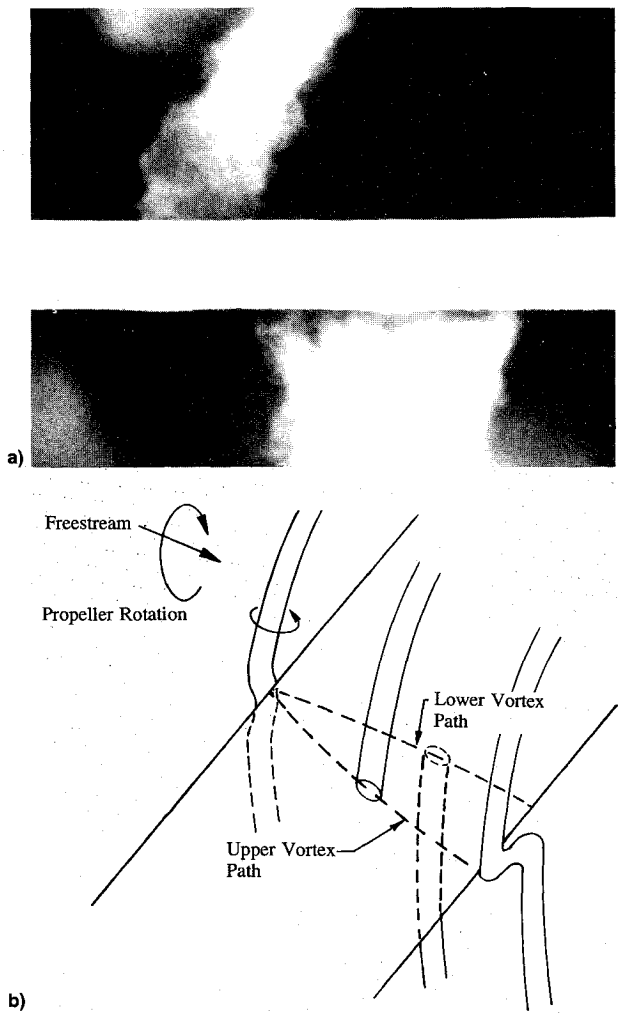

Fig. 4 Spanwise shear of propeller tip vortex at the wing trailing edge as viewed from downstream: a) power absorbing condition (J = 0.9, wing AOA = 5 deg, pitch = 16 deg); b) graphical representation.

wing trailing edge showed evidence of a horizontal vortex filament joining the previously severed ends.[15]

Flow Visualization Discussion

The direction of the spanwise shear observed during flow visualization in the propeller rotation-up region under powered conditions agrees with the predictions of Ribner and Ellis.[23] Numerically calculated spanwise displacements on the rotation-down side were predicted to be small, and no spanwise motion was measurable using the present experimental method.

Two possible mechanisms for the spanwise shear of the helical propeller tip vortex have been identified: 1) an image vortex effect, and 2) a spanwise wing circulation gradient. The image vortex effect is seen when considering a spanwise section (plane) perpendicular to the wing (see Fig. 5). The helical vortex segment in this plane now looks like a two-dimensional vortex near a surface. The vortex will move according to the direction imposed by the image vortex. When the helix was cut on the rotation-up side, the helix angled in an upstream direction. When the helix is cut on the rotation-down side, the helix is angled in a downstream direction. At 0-deg wing AOA this angle was of the same magnitude on both sides of the center of rotation as that measured from the perpendicular to the wing chord line. As wing AOA increased, this angle between the perpendicular to the wing and the vortex filament increased in magnitude on the rotation-up side and decreased in magnitude on the rotation-down

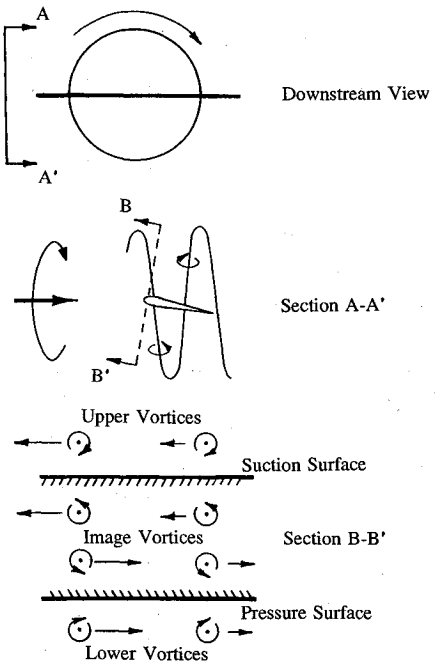

Fig. 5 Image vortex mechanism of spanwise tip vortex motion for a propeller power absorbing condition.

side. This explains the exaggerated spanwise shearing on the rotation-up side at the maximum AOA. By measuring the angle of the helix from photographs, this upstream/downstream angle of the helix was found to be 16.5 ± 1.3 deg from vertical in the power-absorbing propeller condition and 10.2 ± 1.0 deg from vertical in the power-output condition. The sign of these angles depend on the side of the propeller from which these angles are measured. A second possible mechanism of spanwise tip vortex motion is due to changes in the spanwise wing lift or circulation. The effect of the propeller wake (swirl and axial velocity) yielded changes in wing circulation. These changes in wing circulation can be thought of as line vortices emanating from the wing. These vortices give rise to spanwise velocities and, hence, propeller tip vortex motion. Since both of these mechanisms act simultaneously, they can add or subtract depending on magnitudes and direction.

The reconnection of the vortex after passing the airfoil was not easily photographed. It was possible to see that the helix did not recover from the distortion, for the tip vortex on the propeller rotation-up side remained misaligned in a spanwise direction, while in the test section (approximately 2.5 m) for the wing at positive AOA. A plausible explanation for the rejoining of the severed filament is that vorticity shed from the wing trailing edge, due to the unsteady loading experience by the wing, acts to joint the vortex filaments.

Unsteady Wing Surface Pressure Measurements

The results of the unsteady wing pressure study are presented with the spanwise coordinates normalized by the propeller radius, as shown in Fig. 1. In order to present the large magnitude of data obtained during testing, line plots at constant spanwise locations and contour plots at constant chordwise position showing the spanwise pressure distribution as a function of nondimensionalized time, have been prepared.

One method used to interpret the unsteady wing surface pressures was to plot the pressure as a function of time for one or more channels at a constant spanwise location. Figure 6 shows a pressure trace for one revolution (no averaging), the ensemble-averaged pressure trace, and the root-mean-square (rms) of the ensemble-averaged trace at one channel. The relatively large rms value in the vicinity of the tip vortex

is due to variations in the position of the core between traces. This phenomenon is known as vortex "jitter" and is expected in vortex interactions. Dittmar and Hall[24] show several examples of this vortex-to-vortex variation in pressure. Video tapes taken during the flow visualization phase of this experiment also revealed this revolution-to-revolution variation of the vortex core position on the wing.

Pressure contours were obtained by plotting pressure as a function of time at each spanwise location. A typical grid for the pressure measurements was 16 chordwise locations and up to 54 spanwise locations. The vortex core position was determined prior to the measurements being recorded, and the spanwise grid spacing was 1.59 mm through this region. Contour plots are presented from channels 1 and 16 at 10-deg AOA (Figs. 7 and 8). Measurements were also obtained with the wing at 0- and 5-deg AOA, but these followed similar trends to those presented, so they were not included. The pressure contour scale was fixed so that the colors in Figs. 7 and 8 correspond to a particular pressure range.

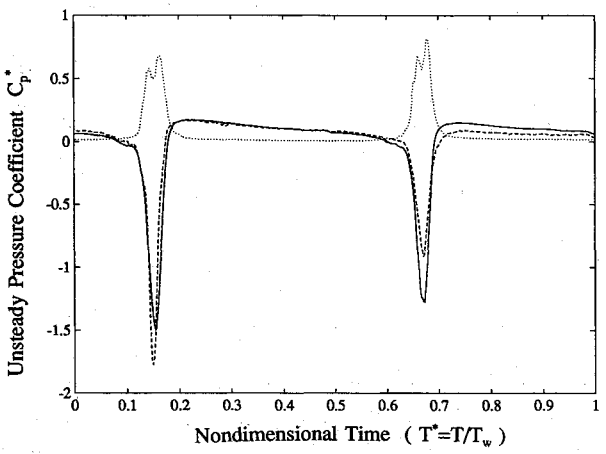

Fig. 6 Plot of a single trace (dashed), the ensemble average (solid), and the rms (dotted) of the ensemble average at channel 2 (X/C = 0.103, r/R = −0.985, AOA = 0 deg, J = 0.37).

A prevalent feature of the propeller wake while passing the wing was that the magnitude of the vortex core pressure decreased as the vortex proceeded along the chord. A reason for this decrease in pressure is that the circumferential velocity in the vortex core locally decreased with distance traveled on the wing due to viscous action at the wing surface. The decrease in the magnitude of the low-pressure region in the viscous blade wake as it proceeded along the wing chord was attributed to viscous dissipation of the velocities in the blade wake at the wing surface. Another apparent feature was that a region of positive pressure followed each low-pressure vortex core region. That a positive pressure region following the vortex core appeared at all angles of attack agreed with previously published data.[24] Thirdly, the vortex core was seen to be elongated in the spanwise direction at the first transducer, and it became more circular as it progressed along the airfoil (Figs. 7 and 8). The vortex rotation was such that the vortex core moved outboard at the leading edge on both the rotation-up side and rotation-down side due to an image vortex effect. This outboard motion at the leading edge was evidence of an inviscid interaction between the tip vortex and the leading edge. The direction of motion at the leading edge was opposite to that photographed for a power absorbing condi-

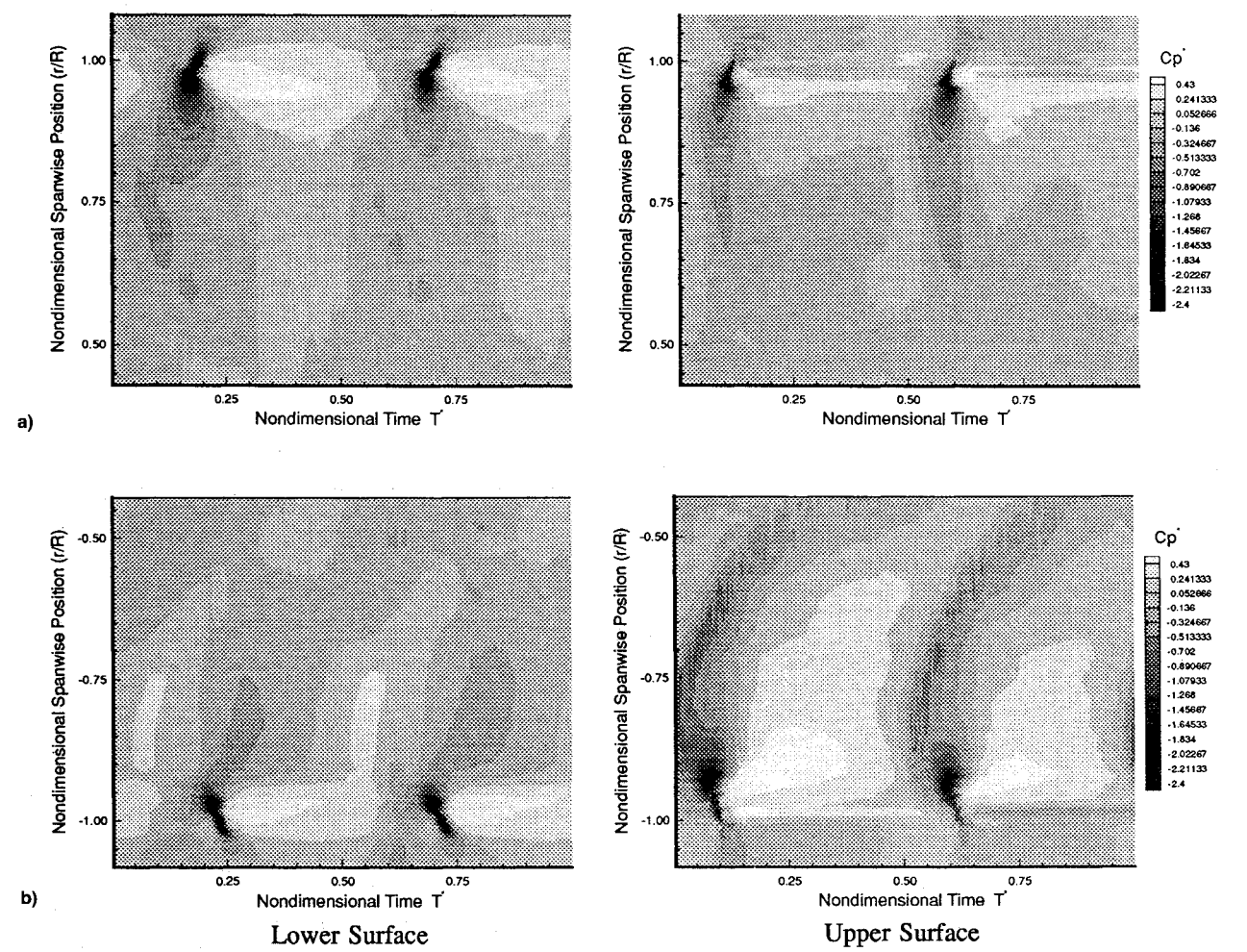

Fig. 7 Wing surface pressure contours at channel 1 (X/C = 0.04, AOA = 10 deg, J = 0.37): a) $r/R > 0.0$, b) $r/R < 0.0$.

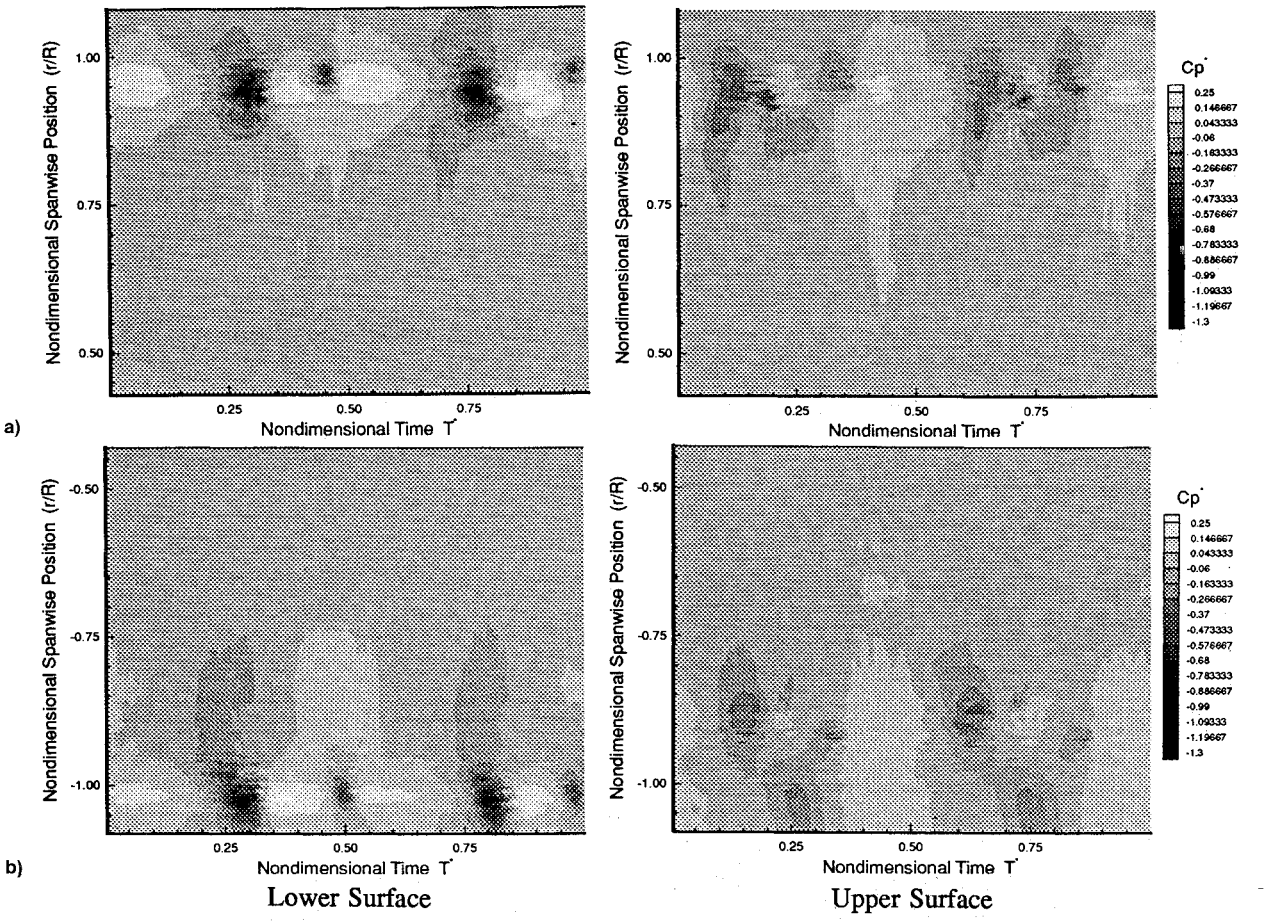

Fig. 8 Wing surface pressure contours at channel 16 (X/C = 0.97, AOA = 10 deg, J = 0.37): a) $r/R > 0.0$, b) $r/R < 0.0$.

tion because the vortex rotation changes for a power output condition. Apparent at channel 1 (X/C = 0.04) was the crescent-shaped low-pressure region due to the blade wake (Fig. 7). The crescent shape resulted because the wake just inboard of the tip vortex reached the wing earlier due to the higher axial velocity inboard of the propeller tip vortex.[25,26] At channel 8 (X/C = 0.48) a small low-pressure region preceded the tip vortex possibly due to an unsteady flow-separation. An increase in the rms of the signal at the location of the secondary low-pressure region supports the theory of a separation bubble. Another anomaly was the occurrence of a second region of low pressure at the trailing edge (channel 16, X/C = 0.97). This secondary low-pressure region is associated with the vortex reconnection at the trailing edge (see Fig. 8).

The magnitude of the pressure in the blade wake depended on whether the measurements were taken on the advancing-blade side or retreating-blade side of the wing. The dependence on blade orientation can be observed in the contour plot for channel 1 (see Fig. 7). This effect was attributed to the tangential velocity in the viscous wake. Tangential velocity was a result of the viscous action at the propeller blade surface. The flow toward the wing surface created a local increase in pressure on the advancing-blade side of the wing due to a stagnating effect; whereas, the flow away from the surface on the retreating-blade side of the airfoil led to a local reduction in the surface pressure.

The spanwise motion of the tip vortex previously observed during the flow visualization phase of this research was verified by measuring the average spanwise location of the tip vortex from pressure contour plots. Figure 9 shows the spanwise motion of the tip vortex on the upper and lower surfaces as a function of AOA. As previously mentioned, the angle between the vortex filament and a perpendicular to the wing creates an image vortex effect. At 0-deg AOA the magnitude of the fore-aft angle between the helical vortex and the per-

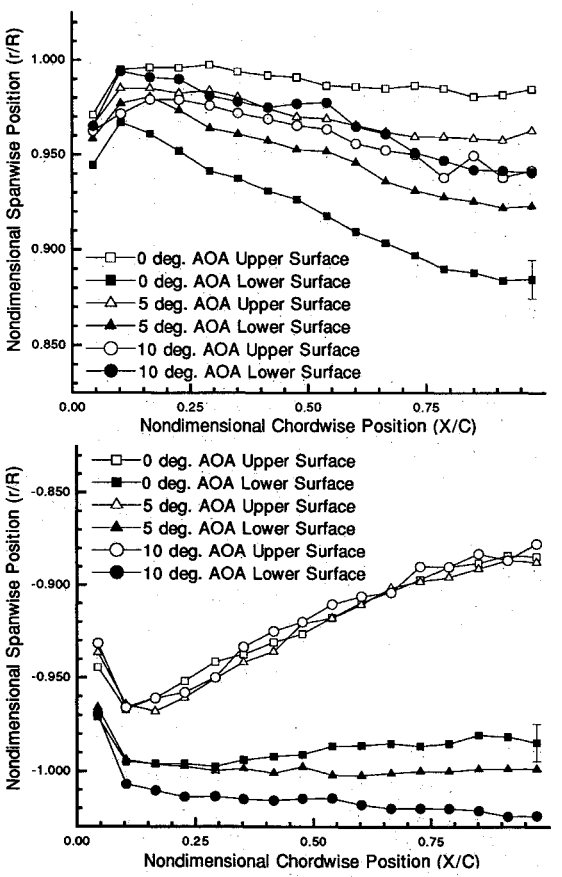

Fig. 9 Vortex trajectories on the wing surface measured from unsteady pressure contour plots: a) $r/R > 0$, b) $r/R < 0$.

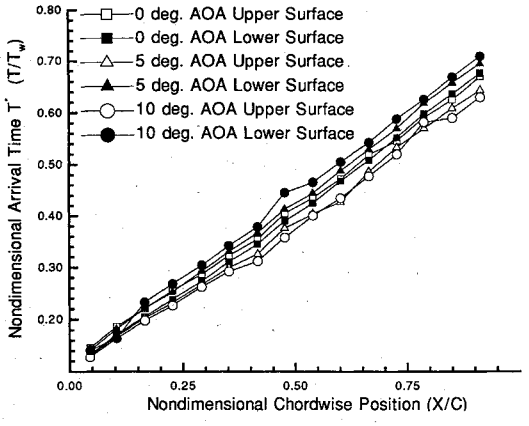

Fig. 10 Vortex chordwise motion on the wing surface measured from unsteady pressure contour plots ($r/R > 0$).

pendicular to the wing chord was measured as 10.2 ± 1.0 deg. As the AOA increased, the angle between a perpendicular to the wing and the vortex filament being cut increased on the rotation-up side and decreased on the rotation-down side. This explains why the upper and lower vortex trajectories diverged on the rotation-up side and converged on the rotation-down side as AOA increased. At 10-deg wing AOA on the rotation-down side, the angle between the perpendicular to the wing and the vortex was approximately zero; therefore, the upper and lower vortex paths were similar. All vortex trajectories were seen to be displaced in the outboard direction at the first transducer regardless of the wing AOA. This leading-edge distortion of the vortex trajectories was attributed to the image vortex effect.

Chordwise motion of the tip vortex is shown in Fig. 10. The slopes of these curves are proportional to the tip vortex speed on the wing surface. Calculation of tip vortex speeds allowed correction of these values to account for small changes in the axial position of the wing due to changing wing AOA. At 0-deg AOA the tip vortex stays well-aligned since the arrival times are the same. As the AOA is increased, the chordwise misalignment increases with the upper surface vortex propagating at a higher speed. This is expected because the flow velocity over a lifting wing should be higher than the flow velocity under the wing.

Conclusions

This investigation into the unsteady nature of propeller/wing aerodynamic interactions revealed a number of new details. An inviscid interaction occurred at the leading edge causing a local deformation of the propeller tip vortex. Viscous action at the wing leading edge severed the propeller tip vortex. Spanwise motion of the propeller tip vortex was observed, and an image vortex effect was used to explain the results. The spanwise motion of the upper and lower vortices diverged on the rotation-up side and converged on the rotation-down side as AOA increased. At a 10-deg wing AOA on the rotation-down side, the angle between the perpendicular to the wing and the vortex was approximately zero; thus, the resultant upper and lower vortex paths were similar. Chordwise vortex speed on the wing is the same above and below a wing at 0-deg AOA. Chordwise motion of the tip vortex over the wing is faster over a lifting wing than below the wing. Due to viscous action at the wing surface, the magnitude of the vortex core pressure and blade wake pressure decreased as the propeller tip vortex proceeded along the chord. A crescent-shaped low-pressure region was observed and was a result of the viscous blade wake. The crescent shape of the viscous wake was attributed to the axial velocity variation in the propeller wake. A second region of low pressure at the trailing edge followed the tip vortex. The appearance of a region of low pressure trailing the tip vortex at channel 16 was unexpected and was associated with the vortex reconnecting at the trailing edge.

Flow visualization and unsteady wing surface pressures were instrumental in obtaining quantitative information about the propeller wake while passing across a wing. Knowledge about the nature of the unsteady propeller/wing interaction will aid in designing quieter, more efficient propeller propulsion systems.

Acknowledgments

The authors would like to acknowledge the support of the NASA Lewis Research Center in this research, and the Natural Sciences and Engineering Research Council of Canada for R. T. Johnston's Fellowship.

References

[1]Thompson, J. S., Smelt, R., Davison, B., and Smith, F., "Comparison of Pusher and Tractor Propellers Mounted on a Wing," Aeronautical Research Council Reports and Memoranda, R&M 2516, London, England, June 1940, pp. 1–17.

[2]Bober, L. A., and Mitchell, G. A., "Summary of Advanced Methods for Predicting High Speed Propeller Performance," NASA TM 81409, Jan. 1980.

[3]Kroo, I., "Propeller-Wing Integration for Minimum Induced Loss," AIAA Paper 84-2470, Oct. 1984.

[4]Miranda, L. R., and Brennan, J. E., "Aerodynamic Effects of Wingtip-Mounted Propellers and Turbines," AIAA Paper 86-1802, June 1986.

[5]Witkowski, D. P., Lee, A. K. H., and Sullivan, J. P., "Aerodynamic Interaction Between Propellers and Wings," AIAA Paper 88-0665, Jan. 1988.

[6]Witkowski, D. P., Johnston, R. T., and Sullivan, J. P., "Propeller/Wing Interaction," AIAA Paper 89-0535, Jan. 1989.

[7]Witkowski, D. P., "An Experimental Investigation of Aerodynamic Interaction Between Propellers and Wings," M.S. Thesis, Purdue Univ., West Lafayette, IN, Aug. 1988.

[8]Lee, A. K. H., "Computational Investigation of Propeller Wing Interaction," M.S. Thesis, Purdue Univ., West Lafayette, IN, April 1988.

[9]Welge, H. R., Neuhart, D. H., and Dahlin, J. A., "Analysis of Mach Number 0.8 Turboprop Slipstream Wing/Nacelle Interactions," NASA CR-166214, Aug. 1981.

[10]Fratello, G. Favier, D., Maresca, C., and Barbi, C. "Experimental and Numerical Study of the Propeller/Fixed Wing Interaction," AIAA Paper 88-2571, June 1988.

[11]Aljabri, A. S., and Hughes, A. C., "Wind Tunnel Investigation of Propeller Slipstream Interaction with Nacelle/Wing/Flap Combinations," *AGARD Symposium of Aerodynamics and Acoustics of Propellers*, No. 366, Toronto, Canada, Oct. 1984, pp. 21.1–21.10.

[12]Heidelberg, L. J., and Woodward, R. P., "Advanced Turboprop Wing Installation Effects Measured by Unsteady Blade Pressure and Noise," AIAA Paper 87-2719, Oct. 1987.

[13]Johnston, R. T., and Sullivan, J. P., "Propeller Tip Vortex Interactions," AIAA Paper 90-0437, Jan. 1990.

[14]Johnston, R. T., Witkowski, D. P., and Sullivan, J. P., "Experimental Results of a Propeller/Wing Interaction Study," Society for Automotive Engineers Transactions 91-0998, April 1991.

[15]Johnston, R. T., "Unsteady Propeller Wing Interactions," Ph.D. Dissertation, Purdue Univ., West Lafayette, IN, Dec. 1991.

[16]Johnston, R. T., and Sullivan, J. P., "Unsteady Wing Surface Pressures in the Wake of a Propeller," AIAA Paper 92-0277, Jan. 1992.

[17]Ward, J. F., and Young, W. H., "A Summary of Current Research in Rotor Unsteady Aerodynamics with Emphasis on Work at Langley Research Center," *Aerodynamics of Rotary Wings*, AGARD CP 111, Marseilles, France, Sept. 1972, pp. 10.1–10.16.

[18]Rorke, J. B., Moffit, R. C., and Ward, J. F., "Wind Tunnel Simulation of Full Scale Vortices," American Helicopter Society Preprint 623, Washington, DC, May 1972.

[19]Behrens, R. D., "An Experimental Investigation of Wind Tunnel Quality," M.S. Thesis, Purdue Univ., West Lafayette, IN, Dec. 1988.

[20]Leehey, P., private communication, Professor of Mechanical Engineering, MIT, Cambridge, MA, 1990.

[21]Kendall, J. M., "Boundary Layer Receptivity to Freestream Turbulence," AIAA Paper 90-1504, June 1990.

[22]Quackenbush, T. R., and Bliss, D. B., "Free Wake Calculation of Rotor Flow Fields for Interactional Aerodynamics," *44th Annual Forum of the American Helicopter Society*, Washington, DC, June 1988, pp. 29–43.

[23]Ribner, H. S., and Ellis, N. D., "Aerodynamics of Wing-Slipstream Interaction," *CASI Transactions*, Vol. 5, No. 2, 1972, pp. 56–63.

[24]Dittmar, J. H., and Hall, D. G., "The Effect of Swirl Recovery Vanes on the Cruise Noise of an Advanced Propeller," AIAA Paper 90-3932, Oct. 1990.

[25]Sundar, R. M., and Sullivan, J. P., "An Experimental Investigation of Propeller Wakes Using a Laser Doppler Velocimeter," AIAA Paper 86-0080, Jan. 1986.

[26]Sundar, R. M., "An Experimental Investigation of Propeller Wakes Using a Laser Velocimeter," Ph.D. Dissertation, Purdue Univ., West Lafayette, IN, Dec. 1980.